Title

ALKBH5 regulates anti–PD-1 therapy response by modulating lactate and suppressive immune cell accumulation in tumor microenvironment

Journal

Proceedings of the National Academy of Sciences of the United States of America, 117(33)

ISSN

0027-8424

Authors

Li, Na
Kang, Yuqi
Wang, Lingling
et al.

Publication Date

2020-08-18

DOI

10.1073/pnas.1918986117

Peer reviewed

ALKBH5 regulates anti–PD-1 therapy response by modulating lactate and suppressive immune cell accumulation in tumor microenvironment

Na Li[a], Yuqi Kang[a,b], Lingling Wang[a], Sarah Huff[a], Rachel Tang[a], Hui Hui[a,b], Kriti Agrawal[a,b], Gwendolyn Michelle Gonzalez[c,d], Yinsheng Wang[c,d], Sandip Pravin Patel[e], and Tariq M. Rana[a,e,1]

[a]Division of Genetics, Department of Pediatrics, Program in Immunology, Institute for Genomic Medicine, University of California San Diego, La Jolla, CA 92093; [b]Bioinformatics Program, University of California San Diego, La Jolla, CA 92093; [c]Environmental Toxicology Graduate Program, University of California, Riverside, CA 92521; [d]Department of Chemistry, University of California, Riverside, CA 92521; and [e]San Diego Center for Precision Immunotherapy, Moores Cancer Center, University of California San Diego, La Jolla, CA 92093

Edited by Stephen P. Goff, Columbia University Medical Center, New York, NY, and approved July 7, 2020 (received for review October 31, 2019)

Although immune checkpoint blockade (ICB) therapy has revolutionized cancer treatment, many patients do not respond or develop resistance to ICB. N^6-methylation of adenosine (m^6A) in RNA regulates many pathophysiological processes. Here, we show that deletion of the m^6A demethylase Alkbh5 sensitized tumors to cancer immunotherapy. Alkbh5 has effects on m^6A density and splicing events in tumors during ICB. Alkbh5 modulates Mct4/Slc16a3 expression and lactate content of the tumor microenvironment and the composition of tumor-infiltrating Treg and myeloid-derived suppressor cells. Importantly, a small-molecule Alkbh5 inhibitor enhanced the efficacy of cancer immunotherapy. Notably, the ALKBH5 gene mutation and expression status of melanoma patients correlate with their response to immunotherapy. Our results suggest that m^6A demethylases in tumor cells contribute to the efficacy of immunotherapy and identify ALKBH5 as a potential therapeutic target to enhance immunotherapy outcome in melanoma, colorectal, and potentially other cancers.

m^6A RNA modification | melanoma | PD-1 blockade | immunotherapy enhancers | GVAX

The adaptive immune response is tightly regulated through immune checkpoint pathways that serve to inhibit T cell activation, thereby maintaining self-tolerance and preventing autoimmunity. The two major checkpoints involve interactions between cytotoxic T lymphocyte antigen 4 (CTLA-4) and programmed cell death protein 1 (PD-1) on T cells and their ligands CD80/CD86 and PD-L1, respectively, which are expressed on various immune cells under physiological conditions. However, expression of these proteins on tumor cells inhibits the T cell activation and enables immune evasion and tumor cell survival. The development of antibodies (Abs) and fusion proteins against PD-1, PD-L1, and CTLA-4, which block negative signaling and enhance the T cell response to tumor antigens, has proven to be a breakthrough in the treatment of solid tumors. Nevertheless, such immune checkpoint blockade (ICB) is ineffective against some tumor types, and many patients who initially respond develop resistance and relapse after ICB. Consequently, understanding the mechanisms of tumor sensitivity, evasion, and resistance to ICB is under intense investigation (1). One of the proposed mechanisms for the failure of ICB is ineffective T cell infiltration and activation due to immunosuppressive conditions within the tumor microenvironment (TME). There is thus an urgent need to develop approaches to increase the sensitivity of tumors to ICBs through combination treatment with molecules that convert an immune-suppressive to an immune-active TME.

Epitranscriptomics is an emerging field that seeks to identify and understand chemical modifications in RNA; the enzymes that deposit, remove, and interpret the modifications (writers, erasers, and readers, respectively); and their effects on gene expression via regulation of RNA metabolism, function, and localization (2, 3). N^6-methyladenosine (m^6A) is the most prevalent internal RNA modification in many species, including mammals. In eukaryotic mRNAs, m^6A is abundant in 5′UTRs, 3′ UTRs, and stop codons (4–6). The m^6A modification is catalyzed by a large RNA methyltransferase complex composed of a catalytic subunit METTL3 and its interacting proteins METTL14, a splicing factor (WTAP), a novel protein (KIAA1429), and other as yet unidentified proteins (2, 3). Conversely, removal of m^6A is catalyzed by the RNA demethylases FTO and ALKBH5 (7, 8). In addition, FTO demethylates N^6,2′-O-dimethyladenosine (m^6A_m) to reduce the stability of target mRNAs and small nuclear RNA (snRNA) biogenesis (9, 10). The m^6A RNA reader proteins, YTH domain-containing proteins (e.g., YTHDF1, YTHDF2, and YTHDF3), specifically bind modified RNA and mediate its effects on RNA stability and translation (11, 12).

In addition to the physiological roles of m^6A in regulating RNA metabolism in such crucial processes as stem cell differentiation, circadian rhythms, spermatogenesis, and the stress response (2, 13), increasing evidence supports a pathological role for perturbed m^6A

Significance

N^6-methylation of adenosine (m^6A) RNA modification plays important roles in development and tumorigenesis. The functions and mechanisms of m^6A demethylases during cancer immunotherapy is still unclear. Here we employed melanoma and colon syngeneic mouse models to study the roles of m^6A demethylases ALKBH5 and FTO during anti–PD-1 antibody and GVAX vaccination therapy. We found that ALKBH5 knockout in tumor cells enhances efficacy of immunotherapy and prolonged mouse survival. ALKBH5 modulates target gene expression and gene splicing, leading to changes of metabolite contents, such as lactate in tumor microenvironment, which regulates suppressive lymphocytes Treg and myeloid-derived suppressor cell accumulations. Importantly, by using ALKBH5-specific inhibitor, we observed the similar phenotype, indicating future translational application of our findings.

Author contributions: T.M.R. conceived and planned the project; N.L. and T.M.R. designed research; N.L., L.W., S.H., R.T., and G.M.G. performed research; S.P.P. contributed new reagents/analytic tools; N.L., Y.K., H.H., K.A., Y.W., S.P.P., and T.M.R. analyzed data; and N.L. and T.M.R. wrote the paper.

T.M.R. is a founder of ViRx Pharmaceuticals and has an equity interest in the company. The terms of this arrangement have been reviewed and approved by the University of California San Diego in accordance with its conflict of interest policies.

This article is a PNAS Direct Submission.

[1]To whom correspondence may be addressed. Email: trana@ucsd.edu.

This article contains supporting information online at https://www.pnas.org/lookup/suppl/doi:10.1073/pnas.1918986117/-/DCSupplemental.

First published August 3, 2020.

metabolism in several disease states. For example, recent studies have shown that the m^{6}A status of mRNA is involved in the regulation of T cell homeostasis (14), viral infection (15), and cancer (16–21).

Here, we employed well-established ICB mouse models of melanoma and colorectal carcinoma to investigate the roles of tumor cell intrinsic Alkbh5 and Fto functions in modulating the response to immunotherapy. We found that CRISPR-mediated deletion of Alkbh5 or Fto in the B16 mouse melanoma (22) or CT26 colorectal carcinoma (23–25) cell line had no effect on tumor growth in untreated mice, but Alkbh5 knockout (KO) significantly reduced tumor growth and prolonged mouse survival during immunotherapy. Alkbh5 deficiency altered immune cell infiltration and metabolite composition in the TME. In addition, the efficacy of cancer immunotherapy was enhanced by pharmacological inhibition of Alkbh5. Finally, we show that gene mutation or down-regulation of the ALKBH5 in melanoma patients correlates with a positive response to PD-1 blockade with pembrolizumab or nivolumab. Thus, our results identify a major role for tumor m^{6}A demethylase in controlling the efficacy of immunotherapy and suggest that combination treatment with ALKBH5 inhibitors may be an approach to sensitize immunotherapy or to overcome tumor resistance to ICB.

Results

Deletion of the m^{6}A RNA Demethylase Alkbh5 Enhances the Efficacy of Anti–PD-1 Treatment. To determine the role of m^{6}A demethylation enzymes in tumor cells in the response to anti–PD-1

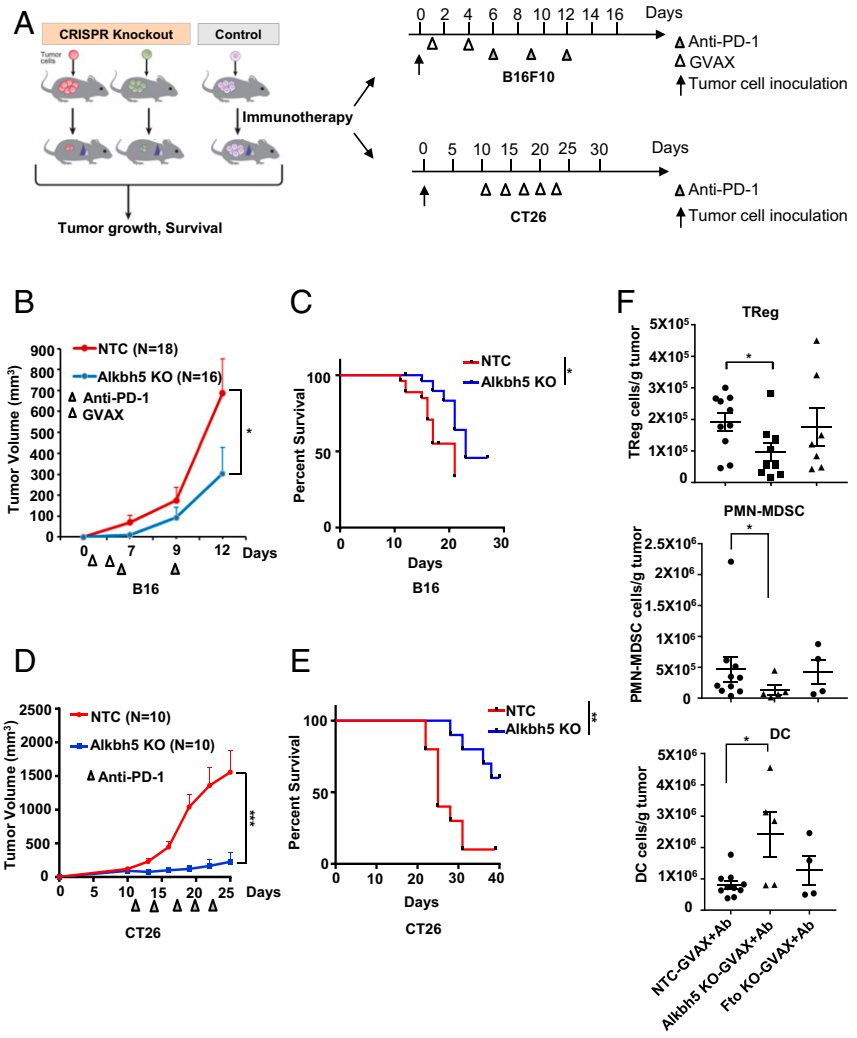

Fig. 1. Deletion of the m^{6}A RNA demethylase Alkbh5 sensitizes tumors to anti–PD-1 immunotherapy and alters immune cell recruitment. (*A*) Experimental design to investigate the role of m^{6}A RNA methylation in anti–PD-1 therapy. Alkbh5 and Fto were deleted by CRISPR/Cas9 editing of B16 mouse melanoma cells and injected subcutaneously into C57BL/6 wild-type mice (5×10^5 per mouse). Control mice received NTC B16 cells. Because B16 cells are poorly immunogenic, all mice were injected subcutaneously with GVAX (irradiated B16 GM-CSF cells) on days 1 and 4 to elicit an anti-B16 immune response. Anti–PD-1 Ab (200 μg per mouse) was injected intraperitoneally on days 6, 9, and 12 (or as indicated for individual experiments). Similar experiments were performed for CT26 cells. The cells were inoculated in BALB/c mice and mice were treated with PD-1 Ab on days 11, 14, 17, 20, and 23. (*B*) Growth of NTC and Alkbh5-KO B16 tumors in C57BL/6 mice treated as described in *A*. Data are the mean ± SEM of the indicated total number of mice per group. For each gene, three B16 CRISPR cell lines with ≥4 mice per line were examined. (*C*) Kaplan–Meier survival curves for mice injected with NTC and Alkbh5-KO B16 cells and treated with GVAX and PD-1 Ab. NTC: $n = 27$; Alkbh5-KO: $n = 28$. Mice were killed and considered "dead" when the tumor size reached 2 cm at the longest axis. (*D*) Growth of NTC and Alkbh5-KO CT26 tumors in BALB/c mice treated with anti–PD-1 Ab. Data are the mean ± SEM of the indicated total number of mice per group. (*E*) Kaplan–Meier survival curves for mice injected with NTC and Alkbh5-KO CT26 cells and treated as described for *D*. NTC: $n = 10$; Alkbh5-KO: $n = 10$. Mice were killed and considered "dead" when the tumor size reached 2 cm at the longest axis. (*F*) FACS quantification of immune cells isolated from B16 NTC, Alkbh5-KO, and Fto-KO tumors as described in *A*. Tumor-infiltrating cells were analyzed using the gating strategies described in *SI Appendix*, Fig. S2 *A*–*C*. CD4$^+$ FoxP3$^+$ (Treg), CD45$^+$CD11b$^+$Ly6G$^+$Ly6CloF4/80$^-$MHC-II$^-$ (PMN-MDSCs), and CD45$^+$Ly6C$^-$MHC-II$^+$ CD24^{hi} F4/80^{lo} (DCs) were analyzed. Data are presented as the mean ± SEM. Points represent individual mice. See also *SI Appendix*, Figs. S1 and S2. *$P < 0.05$, **$P < 0.01$, ***$P < 0.001$.

therapy, we employed a mouse model using the poorly immunogenic murine melanoma cell line B16 or modestly immunogenic colorectal cancer cell line CT26. In the standard protocol (Fig. 1*A*), B16 cells were deleted of Alkbh5 or Fto by CRISPR/Cas9 editing and subcutaneously injected into wild-type syngeneic C57BL/6 mice, which were then vaccinated on days 1 and 4 with GVAX (26), composed of irradiated B16 cells secreting granulocyte-macrophage colony-stimulating factor (GM-CSF) to induce an antitumor T cell response. The mice were then treated with anti–PD-1 Ab on days 6, 9, and 12 (or as indicated for individual experiments). In the CT26 model, control or KO cells were subcutaneously injected into BALB/c mice, and mice were then treated with anti–PD-1 Ab on days 11, 14, 17, 20, and 23 (Fig. 1*A*). Gene editing was performed with up to four distinct Alkbh5- or Fto-targeting single-guide RNAs (sgRNAs) per gene (or nontargeting control sgRNAs, NTC), and B16 lines with complete deletion were selected for further experiments (*SI Appendix*, Fig. S1 *A* and *B*). Compared with NTC-B16 tumors, growth of Alkbh5-KO and Fto-KO tumors was significantly reduced by GVAX/anti–PD-1 treatment (Fig. 1*B* and *SI Appendix*, Fig. S1 *C* and *G–I*) and the survival of Alkbh5- but not Fto-deficient tumor-bearing mice was significantly prolonged (Fig. 1*C* and *SI Appendix*, Fig. S1*D*).

We then sought to determine whether the effects of Alkbh5 and Fto KO reflect a generalizable phenomenon during cancer immunotherapy. For this purpose, we employed a modestly immunogenic colorectal cancer line CT26, which responds to PD-1 Ab treatment (23–25). Similar to the B16 model, we found the tumor growth of Alkbh5 KO was significantly reduced compared with NTC in CT26 tumors treated with PD-1 Ab. However, Fto-KO tumors did not show significant changes although they grew slower than NTC (Fig. 1*D* and *SI Appendix*, Fig. S1 *E* and *J–L*). As observed in the B16 model, the survival of Alkbh5-deficient tumor-bearing mice were significantly prolonged in CT26 model (Fig. 1*E* and *SI Appendix*, Fig. S1*F*). These data confirmed the role of Alkbh5-KO and Fto-KO tumors in immunotherapy independent of tumor types. Alkbh5 KO showed more dramatic effects than Fto KO in restricting tumor growth and prolonging mouse survival. In addition, there were no significant differences between the growth of NTC, Alkbh5-KO, and Fto-KO B16 cells either in vitro (*SI Appendix*, Fig. S1*M*) or in vivo in untreated mice (*SI Appendix*, Fig. S1 *N* and *O*), indicating that deletion of the m^{6}A demethylases did not intrinsically impair their growth. Taken together, these data demonstrate that Alkbh5 expression is not required for their growth or survival in vitro or in vivo; however, the enzymes play a crucial role in the efficacy of anti–PD-1 therapy.

Deletion of Alkbh5 in Melanoma Cells Alters the Recruitment of Immune Cell Subpopulations during GVAX/Anti–PD-1 Treatment. To examine the mechanism by which Alkbh5 modulates GVAX/anti–PD-1 therapy, we examined whether Alkbh5 and Fto deletion in tumor cells modulates immune cell recruitment during GVAX/anti–PD-1 therapy by flow cytometric analysis of tumor infiltrates on day 12 (*SI Appendix*, Fig. S2 *A–C*). Compared with NTC B16 tumors, there is no significant difference in total number of tumor infiltrated lymphocytes (CD45$^+$), CD4$^+$, CD8$^+$ cells in Alkbh5- and Fto-deficient mouse tumors, although a trend to higher abundance of granzyme B (GZMB)$^+$ CD8, GZMB$^+$ CD4 T cell, and NK cell numbers in *Fto*-null mice tumor (*SI Appendix*, Fig. S2*D*). However, the number of infiltrating regulatory T cells (Tregs) and polymorphonuclear myeloid-derived suppressor cells (PMN-MDSCs), but not myeloid (M)-MDSCs, was significantly decreased in Alkbh5-KO tumors compared with NTC tumors during GVAX/anti–PD-1 treatment (Fig. 1*F* and *SI Appendix*, Fig. S2 *D–F*). Interestingly, dendritic cells (DCs), but not macrophages, were also significantly elevated in Alkhb5-KO tumors compared with NTC tumors (Fig. 1*F* and *SI Appendix*, Fig. S2 *D–F*). In contrast, Fto-KO tumors did not show significant changes in MDSC, Tregs, or DC cell populations (Fig. 1*F* and *SI Appendix*, Fig. S2 *D–F*). In accordance with these observations, in Tcra-deficient mice, which lack the TCR-α chain and do not develop mature CD4$^+$ and CD8$^+$ T cells, the effects of Alkbh5 KO but not Fto KO on tumor growth were dampened, but not eliminated (Fig. 2*A* and *SI Appendix*, Fig. S2*G*), suggesting that the effect of Alkbh5 in regulating GVAX/anti–PD-1 therapy was partially independent of the host T cell response. To verify the decrease in PMN-MDSCs, we performed immunohistochemical staining and found a marked reduction in the accumulation of MDSCs in Alkbh5-KO tumors compared with NTC tumors on day 12 (Fig. 2*B*).

Cross-talk between Tregs and other immune cells is an important contributor to tumor-induced immune suppression; for example, MDSCs can induce Treg amplification and decrease DC differentiation in the TME, and Tregs can greatly inhibit cytotoxic T cell function (27). To assess Treg function in GVAX/anti–PD-1 therapy of melanoma, we monitored the effect on tumor growth after injection of a Treg-depleting anti-CD25 Ab on day 11 of treatment (28, 29). We observed that Treg depletion in NTC tumors showed significant decrease in tumor growth (Fig. 2*C*), while Alkbh5-KO tumors, which had lower numbers of Treg cells than NTC tumors (Fig. 1*F*), did not show significant effects on tumor growth (Fig. 2*C*). These data suggest that Treg cells played important roles in the effects of Alkbh5 KO to restrict tumor growth during therapy, since Treg depletion only worked in NTC tumors that had higher Treg cell numbers. Similarly, we also performed MDSC depletion to assess the tumor growth in NTC and Alkbh5-KO tumors during ICB therapy. Our results show that MDSC depletion had an effect similar to Treg depletion while growth kinetics may vary from these deletions in NTC tumors (Fig. 2*D*). Collectively, these data demonstrate that tumor cell expression of Alkbh5 plays an important role in tumor growth by modulating the recruitment of immunosuppressive MDSCs and Tregs during GVAX/anti–PD-1 therapy.

m^{6}A Demethylase Deletion Alters the Tumor Cell Transcriptome during GVAX/Anti–PD-1 Treatment. To understand the regulatory role of Alkbh5 and Fto in tumor therapy at the molecular level, we performed RNA-sequencing (RNA-seq) to identify differentially expressed genes (DEGs) in NTC B16 tumors compared with Alkbh5-KO or Fto-KO tumors on day 12 of GVAX/anti–PD-1 treatment. Tumors were confirmed to be Alkbh5- or Fto-deficient before RNA-seq analysis (*SI Appendix*, Fig. S3 *A* and *B*). Gene ontology (GO) analysis showed that the DEGs in Alkbh5-KO tumors were predominantly involved in metabolic processes, apoptosis, cell adhesion, transport, and hypoxia (Fig. 2*E* and *SI Appendix*, Fig. S3*C*). Interestingly, however, DEGs in Fto-KO tumors were mostly immune response-associated genes (*SI Appendix*, Fig. S3 *D* and *E*). Indeed, further analysis of GO pathways and heatmaps revealed that >80% of the DEGs differed between Alkbh5-KO and Fto-KO B16 tumors. Genes most affected by Alkbh5 KO were associated with regulation of tumor cell survival, adhesion, metastasis, and metabolism, such as Ralgps2, Mmp3, Epha4, Adgrg7, Reln, and Mct4/Slc16a3 (Fig. 2*F*), whereas those most affected by Fto KO were associated with IFN-γ and chemokine signaling, including IRF1, IRF9, STAT2, Cxcl9, Ccl5, and Ccr5 (*SI Appendix*, Fig. S3*F*). To confirm this result, we exposed NTC, Alkbh5-KO, and Fto-KO B16 cells to IFN-γ in vitro and analyzed gene expression by qRT-PCR. As shown in *SI Appendix*, Fig. S3*G*, Fto-KO, but not Alkbh5-KO or NTC tumor cells showed increased expression of the IFN-γ pathway targets Pdl1 and Irf1 and the chemokines Cxcl9, Cxcl10, and Ccl5 after IFN-γ stimulation. These results suggest that, during anti–PD-1/GVAX therapy, Alkbh5

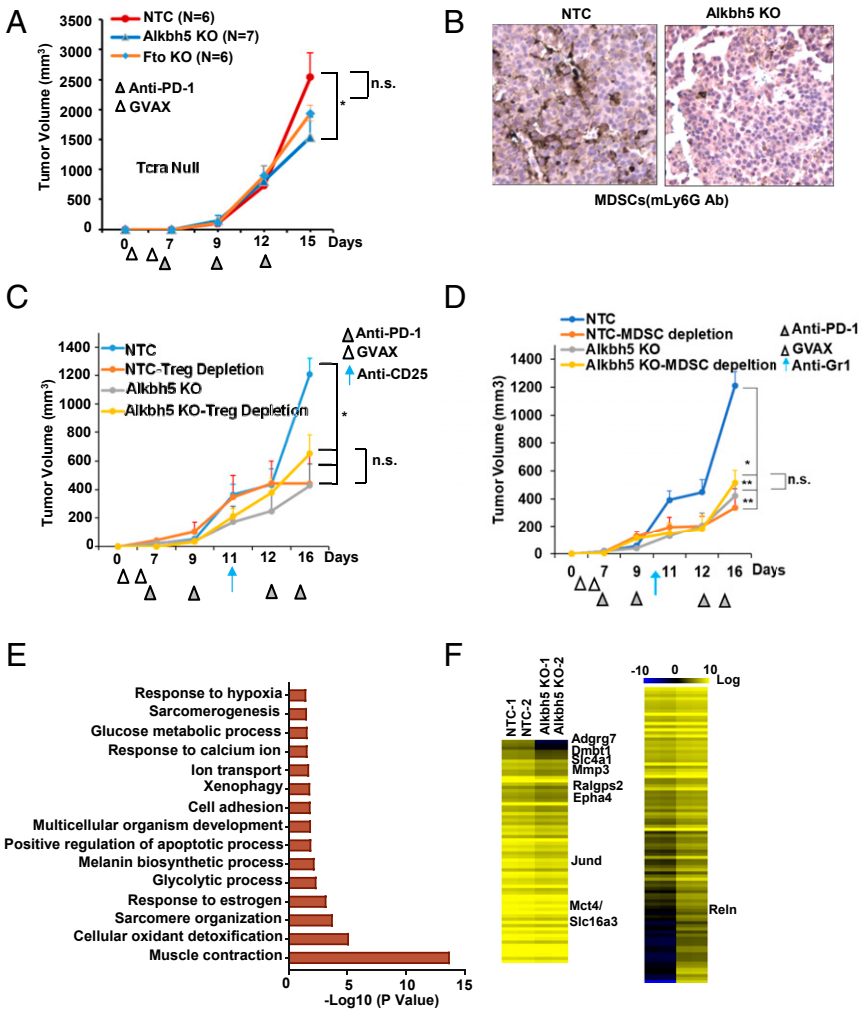

Fig. 2. Alkbh5 regulates tumor infiltration of Treg and MDSCs and gene expression during GVAX/anti–PD-1 therapy. (*A*) As described for Fig. 1*A*, except B16 cells were injected into B6.129S2-Tcra^{tm1Mom}/J (TCR-α–deficient) mice, which are devoid of mature CD8$^+$ and CD4$^+$ T cells. Data are presented as the mean ± SEM. *$P < 0.05$; n.s., not significant. (*B*) Immunohistochemical staining of Ly6G$^+$ PMN-MDSCs in NTC or Alkbh5-KO tumors isolated from mice on day 12. Magnification: 50 μm. (*C*) Growth of NTC and Alkbh5-KO tumors in mice treated as described in Fig. 1*A* and additionally injected intraperitoneally with 10 mg/kg of control IgG or Treg-depleting anti-CD25 Ab on day 11. Data are presented as the mean ± SEM. *$P < 0.05$ vs. NTC control mice. (*D*) Growth of NTC and Alkbh5-KO tumors in mice treated as described in Fig. 1*A* and additionally injected intraperitoneally with 10 mg/kg of control IgG or MDSC-depleting anti-mouse Ly6G/Ly6C (Gr-1) Ab on day 10. Data are presented as the mean ± SEM. *$P < 0.05$, **$P < 0.01$ vs. NTC control mice. (*E* and *F*) GO analysis (*E*) and heatmap presentation (*F*) of DEGs in Alkbh5-KO tumors compared with NTC tumors. Genes satisfying the cut-off criteria of $P < 0.05$ and log fold-change >0.5 or <−0.5 are shown. See also *SI Appendix*, Figs. S2 and S3.

expression in B16 melanoma cells predominantly affects cell intrinsic changes and recruitment of immune cells to the TME, while Fto is involved in regulating IFN-γ and inflammatory chemokine pathways.

IFN-γ pathway activation has been shown to be an important indicator of the efficacy of PD-1 blockade in mouse model studies (22), whereas another study of melanoma patients identified associations between anti–PD-1 response and expression of genes involved in mesenchymal transition, inflammatory, wound healing, and angiogenesis, but not the IFN-γ pathway or other gene signatures indicative of sensitivity to ICB (30). Therefore, we analyzed a gene-expression dataset from 38 melanoma patients who did ($n = 21$) or did not ($n = 17$) respond to anti–PD-1 therapy, and searched for DEGs that were also identified here as DEGs in B16 tumors with Alkbh5 or Fto KO. This analysis identified 8 genes that were commonly down-regulated in Alkbh5-KO B16 tumors and responder melanoma patients, and 11 genes that were commonly down-regulated in Fto-KO B16 tumors and responder patients (*SI Appendix*, Fig. S3 *I* and *K*). Fewer genes were commonly up-regulated between these groups (*SI Appendix*, Fig. S3 *H* and *J*). These results suggest that the down-regulated genes conserved among mouse model and patients receiving PD-1 Ab treatment play important roles in regulating cancer immunotherapy response and are potential target genes of Alkbh5 and Fto.

Alkbh5 Deletion in Melanoma Cells Affects the m^{6}A Epitranscriptome during GVAX/Anti–PD-1 Treatment. Given the profound importance of m^{6}A in regulating the function of target RNAs and gene expression (31, 32), we next examined how Alkbh5 affected m^{6}A content in RNA by LC-MS/MS of B16 tumors on day 12 of GVAX/anti–PD-1 therapy (33–35). This analysis revealed that levels of m^{6}A were significantly increased in Alkbh5-KO but not in Fto-KO tumors (Fig. 3*A*). We then performed m^{6}A RNA immunoprecipitation followed by high-throughput sequencing (MeRIP-seq) to determine whether the altered gene expression observed in the KO tumors was a consequence of m^{6}A/m^{6}Am demethylation. To obtain the most robust data, we selected only

m^{6}A peaks identified by two independent peak calling algorithms and detected in tumors from all biological replicates per group (*SI Appendix*, Fig. S4 *A* and *B*). In the NTC and Fto-KO B16 tumors, the majority of m^{6}A peaks were detected in the coding sequence (CDS) and the 3′UTR and 5′UTR, which is consistent with previous studies (4, 5, 36). Notably, the density of m^{6}A peaks in intronic regions was substantially higher in Alkhb5-KO tumors compared with NTC tumors during treatment (Fig. 3*B*), and Alkbh5-KO tumors had more unique m^{6}A peaks compared with NTC or Fto-KO tumors (Fig. 3*C* and *SI Appendix*, Fig. S4*C*). Analysis of motifs in the m^{6}A peaks showed that the canonical m^{6}A motif DRACH (D = A, G, U; R = A, G; H = A, C, U) was the most common motif in all tumor groups. The putative m^{6}Am motif BCA (B = C, U, or G; A* = methylatable A) was present in other enriched motifs. One motif enriched in Alkbh5-KO tumors contained the SAG core, which is reminiscent of the SRSF binding site motif known to affect gene splicing (Fig. 3*D* and *SI Appendix*, Fig. S4*D*). These data suggest that Fto and Alkbh5 deletion had some common and some distinct effects on m^{6}A/m^{6}Am peaks in B16 tumors, which might contribute to the different mechanisms through which the two demethylases influence the efficacy of GVAX/anti–PD-1 therapy.

We next examined whether the down-regulation of the overlapped genes in Alkbh5-KO or Fto-KO tumors (responding better than NTC) and melanoma patients responding to immunotherapy was due to altered levels of m^{6}A (*SI Appendix*, Fig. S3 *I* and *K*). Five of eight common down-regulated genes had increased m^{6}A peaks in Alkbh5-deficient mouse tumor (shown in red in *SI Appendix*, Fig. S3*I*). While only 1 of a total of 11 common genes, Mex3d, had elevated m^{6}A levels in Fto-deficient tumors (red in *SI Appendix*, Fig. S3*K*). m^{6}A peaks in Mex3d, common in both Alkbh5 and Fto down-regulated genes, increased compared to NTC (*SI Appendix*, Fig. S4*E*). Mct4/Slc16a3, found in only Alkbh5 down-regulated genes, had significantly increased m^{6}A density in the Alkbh5-KO tumors compared to NTC (Fig. 3 *E* and *F*).

These results suggest that Alkbh5 KO increased m^{6}A levels and reduced expression of certain genes involved in immunotherapy resistance. The overall levels of m^{6}A in Fto-deficient tumors was not changed; however, it showed increased m^{6}A at some genes, albeit the number of changed genes were much less than in Alkbh5-KO tumors (e.g., *SI Appendix*, Figs. S3 *I–K* and S4*E*).

m^{6}A Density Is Increased Near Splice Sites and Leads to Aberrant RNA Splicing in Alkbh5-Deficient Tumors. Although the regulatory role of m^{6}A deposition in splicing is somewhat controversial (36, 37), Alkbh5 has been reported to affect splicing in an m^{6}A demethylase-dependent manner (38). Our MeRIP-seq results showed that unique m^{6}A peaks were more prevalent in Alkbh5-KO tumors compared with NTC or Fto-KO tumors during GVAX/anti–PD-1 treatment, and that one m^{6}A motif enriched in Alkbh5-KO tumors had a sequence similar to the SRSF binding motif (Fig. 3 *B–D*) (36). GO analysis of mRNAs with unique m^{6}A peaks in Alkbh5-KO tumors showed enrichment in splicing, cell cycle, and signaling pathway functions (*SI Appendix*, Fig. S5 *A* and *B*), suggesting that Alkbh5 also regulates gene expression in B16 cells through effects on mRNA splicing. To test this hypothesis, we examined the location of m^{6}A at 5′ or 3′ intron–exon splice junctions by positional assessment. Consistent with a previous study using m^{6}A individual nucleotide-resolution cross-linking and immunoprecipitation (36, 37), we found that m^{6}A deposition increased from both 5′ and 3′ splice sites to the internal exonic regions in NTC control tumors with immunotherapy (Fig. 3*G*). Surprisingly, we found that in Alkbh5-deficient tumors, the m^{6}A densities were elevated at the both 5′ and 3′ splice sites, with a dramatic increase at the proximal region to the 3′ splicing site (Fig. 3*G*). In contrast, m^{6}A deposition at splice sites in Fto-KO tumors was comparable to that in NTC tumors (*SI Appendix*, Fig. S5*C*), suggesting that Alkbh5 plays a role in gene splicing through depositing m^{6}A modifications near the splicing sites.

Changes in m^{6}Am by FTO have been reported to affect snRNA biogenesis and gene splicing (10), and we observed an increase in m^{6}Am/m^{6}A in U1, U2, and U3 snRNAs in Fto-KO tumors compared with NTC tumors (*SI Appendix*, Fig. S5*E*). To investigate this further, we analyzed our RNA-seq data using MISO to detect differences in RNA splicing. Although the global splicing profiles were unaffected by Alkbh5 or Fto deletion, the frequency of spliced-in transcripts (as reflected by the percent spliced-in index, PSI) in a subset of genes was increased by Alkbh5 deletion in tumors analyzed during GVAX/anti–PD-1 treatment (Fig. 3*H* and *SI Appendix*, Fig. S5 *D*, *F*, and *G*). Categories of gene functions, where the PSI was changed in Alkbh5-KO tumors, included genes involved in important cellular processes, such as transcription, splicing, protein degradation, transport, translation, and cytokine-related pathways (*SI Appendix*, Fig. S5 *D* and *H*).

To determine whether changes in m^{6}A deposition were linked with mRNA splicing, we next asked whether the m^{6}A density increased in mRNAs with higher spliced-in frequencies (i.e., higher PSI) in Alkbh5-KO compared with NTC tumors. Indeed, mRNA with high PSI due to Alkbh5 KO had higher m^{6}A densities near intron–exon junctions compared with the same mRNAs in NTC tumors; these mRNAs included Usp15, Arid4b, and Eif4a2 (*SI Appendix*, Fig. S5*I*). Among the genes with altered PSI in Alkbh5-KO tumors after immunotherapy, Eif4a2 regulates gene translation, Arid4b regulates gene transcription, and Sema6d, Setd5, and Met regulate vasculature, the expression and secretion of vascular endothelial growth factor, and hepatocyte growth factor, both of which promote MDSC expansion (39–42). Usp15 affects signaling by transforming growth factor-β, which attracts and activates Tregs. Notably, Met and Usp15 are expressed as isoforms that have markedly different functions (43, 44), suggesting that gene-splicing changes may play a role in TME composition and eventually affecting the immunotherapy efficacy. Taken together, these data indicate that Alkbh5 regulates the density of m^{6}A near spice sites in multiple mRNAs with functions potentially important during GVAX/anti–PD-1 therapy.

Alkbh5 Regulates Lactate and Vegfα Accumulation in the TME during GVAX/Anti–PD-1 Treatment. Our findings above suggest that Alkbh5 KO regulates its targets by changing m^{6}A levels, which leads to decreased gene expression or altered gene splicing. Some of these genes are involved in regulating cytokines (Vegfα and Tgfβ1) or metabolite (lactate) in TME, such as Mct4/Slc16a3, Usp15, Met, and Sema6d (Figs. 2*F* and 3 *E* and *F* and *SI Appendix*, Fig. S5 *D* and *H–I*). Therefore, it is important to examine whether in Alkbh5-KO tumors, cytokines, or metabolites in the TME are altered that consequently modulate tumor infiltrated lymphocyte populations and immunotherapy efficacy (Figs. 1 and 2).

To address these questions, we quantified lactate, Vegfα, and Tgfβ1 concentrations in the tumor interstitial fluid (TIF), which contains proteins, metabolites, and other noncellular substances present in the TME (*SI Appendix*, Fig. S6*A*). Indeed, both the lactate concentration in TIF and the total lactate content in the TME were dramatically reduced in Alkbh5-KO tumors compared with NTC tumors (Fig. 4*A*). Although the Vegfα concentration in TIF was comparable between NTC and Alkbh5-KO tumors, the total Vegfα content in the TME was reduced by Alkbh5 deletion (Fig. 4*B*). In agreement with a previous study, we also found that Vegfα levels were much lower in plasma than in TIF (45), showing that our isolation of TIF was successful (*SI Appendix*, Fig. S6*D*). The lactate and Vegfα levels in plasma did

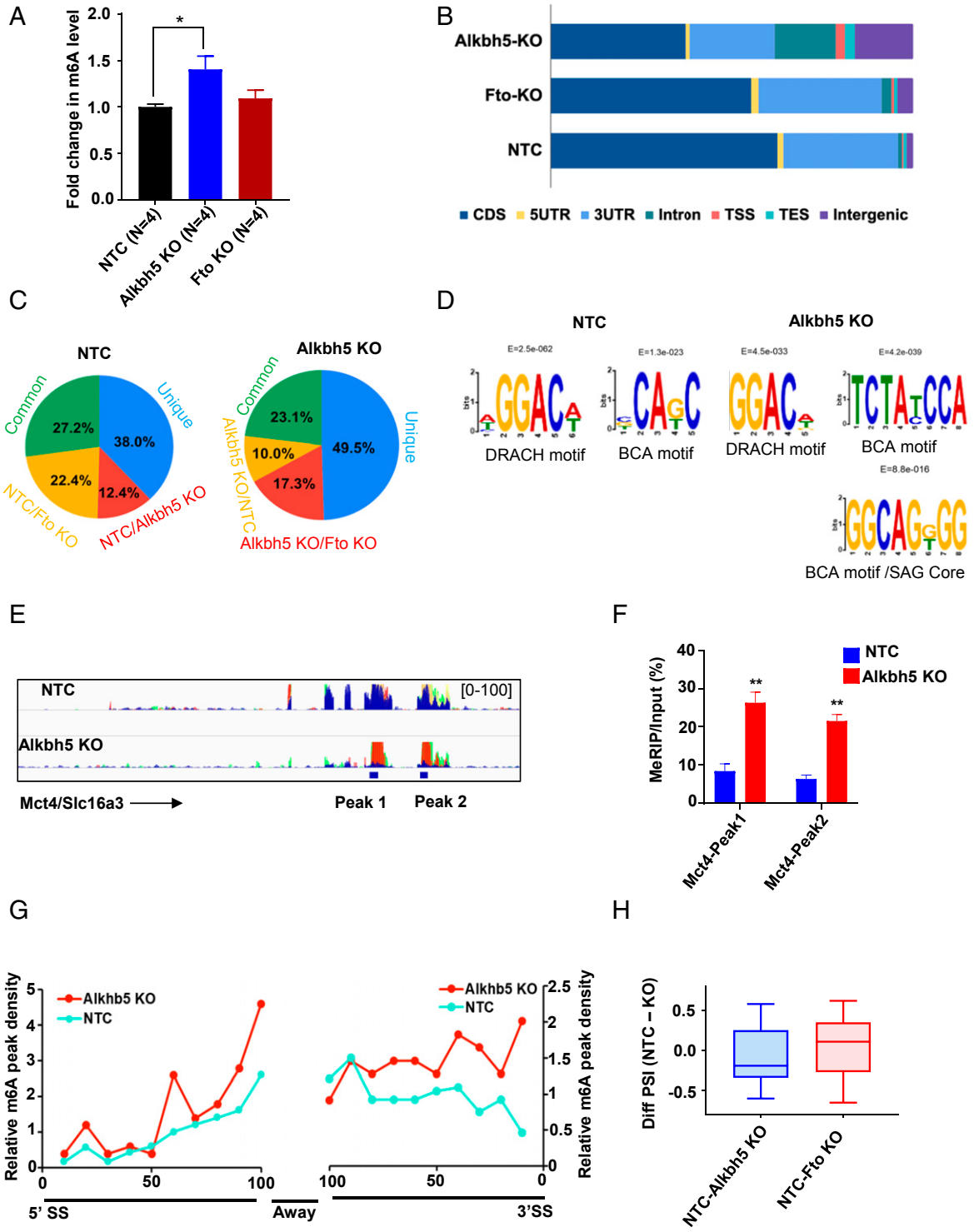

Fig. 3. Alkbh5 regulates gene splicing during GVAX/anti–PD-1 immunotherapy. (*A*) LC-MS/MS quantification of m^{6}A in ribosome-depleted total RNA isolated from NTC, Alkbh5-KO, and Fto-KO tumors. Data are presented as the mean ± SEM fold-change relative to the NTC control in four mice per group. *$P < 0.05$ vs. NTC control. (*B*) Genomic location of the conserved m^{6}A peaks identified by MeRIP-seq in B16 tumors from mice treated as described in Fig. 1*A*. Plot shows the proportion of m^{6}A in the CDS, 5′ and 3′ UTRs, introns, transcription start site (TSS), transcription end site (TES), and intergenic regions. (*C*) Pie charts showing the proportions of common and unique m^{6}A/m^{6}Am peaks of NTC and Alkbh5-KO B16 tumors from mice treated as described in Fig. 1*A*. (*D*) Top consensus motifs of MeRIP-seq peaks identified by MEME in NTC and Alkbh5-KO B16 tumors from mice treated as described in Fig. 1*A*. (*E*) Genome browser tracks of NTC and Alkbh5-KO tumors after treatment were shown for Slc16A3/Mct4 with called m^{6}A sites by MeRIP and corresponding inputs. Input was indicated by blue color in each track. Bed files of the called peaks were shown under the MeRIP track of each group. Scale of the peak density was set the same for all of the groups and shown in the corner. (*F*) MeRIP-qPCR of m^{6}A enrichment in Mct4 gene for both peak 1 and peak 2 regions shown in *E*. **$P < 0.01$ vs. NTC control. (*G*) The density of m^{6}A in the region of 100-nt exon regions from the 5′ splice site ("SS") and the 3′ SS. The relative m^{6}A peak density of a specific position in NTC and Alkbh5-deficient tumors was calculated as the scaled m^{6}A peak density proportional to the average m^{6}A peak density in the internal exonic regions. (*H*) Difference of PSI was calculated by MISO as NTC control minus either Alkbh5-KO or Fto-KO tumors. See also *SI Appendix*, Figs. S4 and S5.

not differ in mice bearing NTC vs. Alkbh5-KO tumors, suggesting that the effect of Alkbh5 deletion on lactate and Vegfα levels was restricted to the TME and was not systemic (*SI Appendix*, Fig. S6 *C* and *D*). In contrast to lactate and Vegfα, we found that the concentration of Tgfβ1 in TIF was increased by Alkbh5 deletion, whereas the TME content of Tgfβ1 was reduced only in Alkbh5-deficient tumors (*SI Appendix*, Fig. S6 *B* and *E*). Collectively, these results showed that Alkbh5 expression in melanoma modulates metabolite and cytokine content with the most significant change of lactate in TIF, suggesting another mechanism by which m^6A demethylase could modulate the infiltration of immune cells during anti–PD-1/GVAX treatment.

Mct4/Slc16a3, an Alkbh5 Target Gene, Is Involved in Regulating Extracellular Lactate Concentration, Tregs, and MDSC Accumulation in the TME. As shown above, we found lactate was the most dramatically decreased metabolite in Alkbh5-KO tumors compared with NTC tumors among all of the Alkbh5-related cytokines and metabolites we examined in the TME (Fig. 4 *A* and *B* and *SI Appendix*, Fig. S6 *A–E*). In Alkbh5-KO tumors, Mct4/Slc16a3 mRNA level was decreased and m^6A density was increased compared with NTC tumors during anti–PD-1/GVAX treatment (Figs. 2*F* and 3 *E* and *F*). Mct4 is a key enzyme catalyzing rapid transport across the plasma membrane of lactate. Lactate is the metabolite that directly affects MDSC and Treg recruitment in tumor sites (46, 47). Therefore, we hypothesized Mct4 is an Alkbh5 target gene in regulating lactate concentration and affecting Tregs and MDSC accumulation in TME during the treatment. To test this hypothesis, we first examined Mct4 expression and RNA stability in NTC and Alkbh5-deficient cells and tumors. We found that Mct4 mRNA levels were lower in Alkbh5-KO than in NTC cells in both B16 and CT26 mouse cell lines, as well as in two other human cell lines when compared ALKBH5 knockdown with control cells (*SI Appendix*, Figs. S6 *F–I* and S9 *B* and *C*). In mouse tumors under anti–PD-1/GVAX treatment, both mRNA and protein levels of Mct4 were decreased in Alkbh5-KO tumors compared with NTC (*SI Appendix*, Fig. S6 *G* and *H*). Next, we performed an mRNA decay assay to determine Mct4 RNA stability in NTC and Alkbh5-KO cells. Our results showed that Mct4 mRNA stability was reduced in Alkbh5-KO cells compared with NTC in both B16 and CT26 cell lines (Fig. 4*C* and *SI Appendix*, Fig. S6 *J–L*). These results strongly suggest that Alkbh5 regulated Mct4 expression by changing its m^6A levels and RNA stability.

To further delineate the role of Mct4 in Alkbh5 KO tumors during anti–PD-1/GVAX treatment, we constructed a stable cell line expressing Mct4 in Alkbh5-KO cells and examined the function of Mct4 in Alkbh5-KO cells in vitro and in vivo. First, we validated the cell lines by detecting the both mRNA and protein levels of Mct4, and performed in vitro proliferation assay for NTC, Alkbh5-KO, and Alkhb5-KO+Mct4 cells. Results of these analyses showed that there was no difference in cell proliferation of NTC, Alkbh5-KO, and Alkbh5-KO+Mct4 cells in vitro (Fig. 4*D* and *SI Appendix*, Fig. S7 *A* and *B*). As Mct4 is a key enzyme mediating transport of lactate across the cell membrane, we examined extracellular lactate concentration in NTC, Alkbh5-KO, and Alkbh5-KO+Mct4 B16 cells. As expected, we observed a reduction of lactate concentration in Alkhb5-KO cells, and an increased level of lactate in Alkhb5-KO+Mct4 cells in vitro (Fig. 4*E*). Furthermore, we inoculated these cells to mice and treated them with anti–PD-1/GVAX and monitored tumor growth in vivo as described above (Fig. 1). We observed a significantly reduced tumor growth in Alkhb5-KO tumors but not Alkbh5-KO+Mct4 tumors compared with NTC, albeit Alkbh5-KO+Mct4 tumors also grew slower than NTC (Fig. 4*F*). These results suggested that Mct4 was one of the major targets of Alkbh5 during anti–PD-1/GVAX treatment. Next, we isolated tumors and assayed the lactate concentration and amounts in TIF and found that lactate levels were significantly reduced in Alkbh5-KO but not Alkbh5-KO+Mct4 tumors, which was consistent with in vitro assay (Fig. 4*G*). In accordance with that, flow cytometry analysis of the tumors showed that Tregs and PMN-MDSC populations were significantly decreased in in Alkbh5-KO but not Alkbh5-KO+Mct4 tumors (Fig. 4 *H* and *I*). Altogether, these results show that Mct4 is a key Alkhb5 target gene mediating reduced lactate levels, as well as Tregs and MDSC populations in Alkbh5-KO tumors during the anti–PD-1/GVAX treatment.

Although not significant, we observed a slower tumor growth in Alkbh5-KO+Mct4 than NTC cells-inoculated mice in vivo (Fig. 4*F*). We speculate that other factors or events also play roles in Alkbh5-KO tumor, albeit not as significant as Mct4, during anti–PD-1/GVAX treatment. Therefore, we analyzed several genes whose splicing events were altered in Alkbh5-KO tumors, and compared their pattens in NTC, Alkbh5-KO, and Alkbh5-KO+Mct4 cells. The results showed that gene splicing changes remained the same in Alkbh5-KO and Alkbh5-KO+Mct4 cells, such as Eif4a2 and Sema6d, suggesting that besides Mct4, they may play roles in Alkbh5-KO tumors (Fig. 4*J* and *SI Appendix*, Fig. S7 *C–E*).

m^6A mRNA Demethylase Activity of Alkbh5 Is Indispensable during GVAX/Anti–PD-1 Treatment. Since Alkbh5 is an m^6A RNA demethylase, we asked whether the m^6A demethylase enzymatic activity is essential for the functions of Alkbh5. We constructed stable cell lines by expressing Alkbh5 CRISPR sgRNA-resistant wild-type or H205A/H267A catalytically inactive mutant [conserved enzymatic sites in human ALKBH5, H204H266 (8, 48)] of Alkhb5 in Alkbh5-KO cells and examined Mct4 expression. Our results showed that wild-type but not mutant Alkbh5 could rescue Mct4 mRNA and protein levels (*SI Appendix*, Fig. S8 *A–D*). We also analyzed gene splicing of Eif4a2 and Sema6d genes, which had altered PSI in Alkbh5-KO tumors, in wild-type and mutant Alkbh5-expressed Alkbh5-KO cell lines. These results showed that Eif4a2 gene splicing was rescued in wild-type but not mutant Alkbh5-expressed Alkbh5-KO cells. MeRIP-seq also showed an increased signal of m^6A in Alkhb5-KO cells compared with NTC in the exon–intron junction, which were involved in the alternative splicing of Eif4a2. On the other hand, gene splicing of Sema6d was not affected by the enzymatic activity of Alkbh5, and we did not observe m^6A peaks around the spliced exons (*SI Appendix*, Fig. S8*E*). These results showed that enzymatic activity of Alkbh5 play important roles in regulating Mct4 RNA and protein expression, as well as certain genes with altered alternative splicing, which was directly affected by m^6A and Alkbh5. Furthermore, we performed in vivo tumor growth experiments in mice treated with GVAX/anti–PD-1. As shown in Fig. 4*K* and *SI Appendix*, Fig. S9*A*, expressing wild-type but not catalytically inactive mutant Alkbh5 in Alkbh5-KO cells abolished the tumor restricting effects of Alkbh5 KO during GVAX/anti–PD-1 treatment. Altogether, these results demonstrate that the catalytic activity of Alkbh5 is indispensable for its effects on in vivo tumor growth during GVAX/anti–PD-1 treatment.

ALKBH5 and MCT4/SLC16A3 Levels in Melanoma Patients Correlate with the Response to Anti–PD-1 Therapy. Our results thus far strongly suggest that ALKBH5 deletion enhances the efficacy of anti–PD-1 therapy. Therefore, we analyzed the Cancer Genome Atlas (TCGA) database to examine the correlation between expression level of ALKBH5 and survival time in metastatic melanoma patients. Consistent with our findings, low expression of ALKBH5 correlated with better patients' survival (Fig. 5*A*). Importantly, Treg cell numbers, as indicated by FOXP3/CD45 ratio, were significant lower in patients with less expression of ALKBH5 (Fig. 5*B*). As described above, we found that Mct4/Slc16a3 was an important Alkbh5 target gene during immunotherapy,

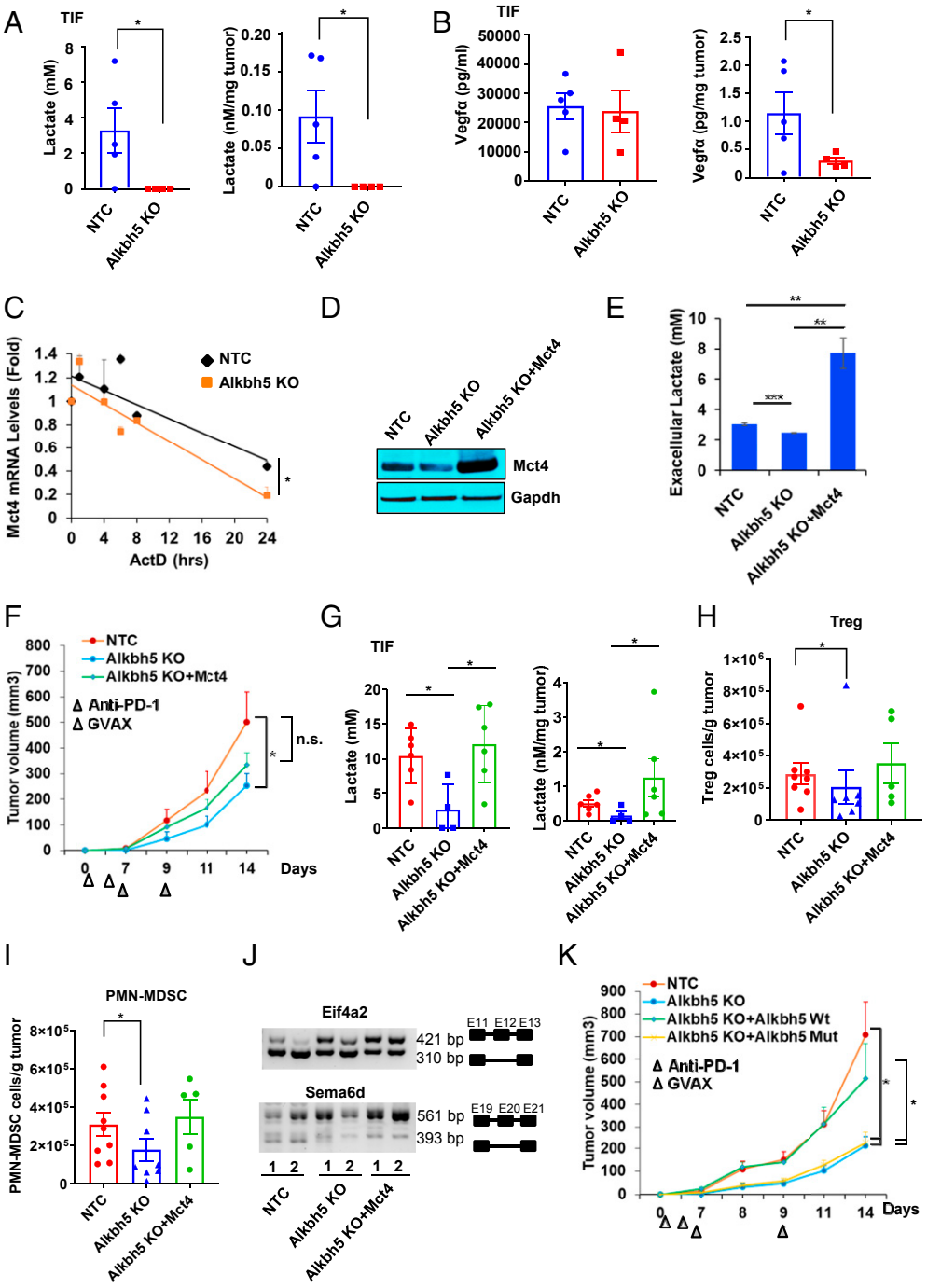

Fig. 4. Mct4/Slc16a3 is an Alkbh5 target gene and regulates lactate contents, Tregs and MDSC accumulation in the TME. (*A*) Lactate concentration and total content in TIF isolated from NTC or Alkbh5-KO tumors excised on day 12 from mice treated as described in Fig. 1*A*. (*Left*) Absolute lactate concentration in TIF; (*Right*) lactate content per milligram tumor. Data are the presented as the mean ± SEM of five (NTC) or four (Alkbh5-KO) mice. (*B*) As for *A*, except Vegfα was analyzed. (*C*) mRNA decay analysis of Mct4/Slc16a3 in NTC and Alkbh5-KO B16 cells. NTC and Alkbh5-KO B16 cells were treated with actinomycin D (ActD) at concentration of 5 μg/mL and cells were collected for RNA extraction at indicated time points. Three independent experiments were performed and calculated. *$P < 0.05$. (*D*) Mct4 protein levels in NTC, Alkbh5-KO, and Alkbh5-KO cells expressing Mct4 (Alkbh5-KO + Mct4) B16 cells by Western blotting. (*E*) Extracellular lactate concentration in supernatants of NTC, Alkbh5-KO, and Alkbh5-KO+Mct4 B16 cells. **$P < 0.01$, ***$P < 0.001$. (*F*) Growth of NTC, Alkbh5-KO, and Alkbh5-KO+Mct4 B16 tumors in C57BL/6 mice treated as described in *A*. Data are the mean ± SEM of the indicated total number of mice per group. The mice number for each group was: NTC: $n = 8$; Alkbh5-KO: $n = 8$; Alkbh5-KO+Mct4: $n = 10$. (*G*) Lactate concentration and total content in TIF isolated from NTC, Alkbh5-KO, and Alkbh5-KO+Mct4 B16 tumors excised on day 12 from mice treated as described in Fig. 1*A*. Data are the presented as the mean ± SEM. Points represent individual mice. *$P < 0.05$. (*H–I*) FACS quantification of immune cells isolated from B16 NTC, Alkbh5-KO, and Alkbh5-KO+Mct4 B16 tumors as described in Fig. 1*A*. Treg cells (*H*) and PMN-MDSC cells (*I*) were analyzed. Data are presented as the mean ± SEM. Points represent individual mice. *$P < 0.05$. (*J*) PCR analysis of alternative splicing of Eif4a2 and Sema6d genes in NTC, Alkbh5-KO, and Alkbh5-KO+Mct4 B16 cells are shown. (*K*) Growth of NTC, Alkbh5-KO, Alkbh5-KO + wild-type Alkbh5 (Alkbh5 KO+Alkbh5 Wt), Alkbh5 KO + catalytically mutant Alkbh5 (Alkbh5 KO+Alkbh5 Mut) tumors in C57BL/6 mice treated as described in Fig. 1*A*. Data are the mean ± SEM of the indicated total number of mice per group. Growth of individual mice are shown in *SI Appendix*, Figs. S9*A*. See also *SI Appendix*, Figs. S6–S9.

and Mct4 level decreased in Alkbh5-KO tumors during therapy. Mct4 is a key gene to mediate lactate secretion which led to reduced lactate in TIF contents and suppressive immune cell populations of Alkhb5-KO tumors during immunotherapy (Figs. 2*F*, 3 *E* and *F*, and 4 *C*–*I*). Therefore, we examined the gene expression of ALKBH5 and MCT4/SLC16A3 in the TCGA database. Consistent with our mouse tumor data, we found there is a positive correlation between ALKBH5 and MCT4/SLC16A3 expression in melanoma patients (Fig. 5*C*). Consistent with our results (Fig. 2 and *SI Appendix*, Fig. S3), our analysis did not show any correlation of ALKBH5 expression with IFN pathway genes IRF1 and PDL1 (*SI Appendix*, Fig. S10 *B* and *C*). We observed a negative correlation of PBRM1 and GZMB, which serves as a positive control for our analysis (49) (*SI Appendix*, Fig. S10*D*).

MCT4/SLC16A3 was also found in the down-regulated gene list of 26 melanoma patients receiving pembrolizumab or nivolumab treatment (30); we then analyzed the percentage of patient response to PD-1 Ab in low- and high-expressed MCT4/SLC16A3 groups. Melanoma patients with low expression of MCT4/SLC16A3 has much higher complete or partial response rate than the high-expression group (Fig. 5*D*). In the same cohort of melanoma patients receiving pembrolizumab or nivolumab treatment, we also observed a positive correlation of ALKBH5 and MCT4/SLC16A3 expression (Fig. 5*E*). We next determined whether melanoma patients harboring ALKBH5 deletion/mutation were more sensitive to anti–PD-1 therapy than patients carrying wild-type ALKBH5. To this end, we examined the treatment response according to their ALKBH5 mutation and gene-expression status. As shown in Fig. 5*F*, we found that more patients harboring deleted or mutated ALKBH5 achieved complete or partial responses to pembrolizumab or nivolumab therapy than did patients with wild-type ALKBH5.

Next, we performed single-cell RNA-seq (scRNA-seq) on tumor cells obtained from a patient with stage IV melanoma who had responded well to anti–PD-1 therapy. By using scRNA-seq, we were able to examine ALKBH5 expression in the resistant tumor cells in patients receiving PD-1 Ab. We identified 10 cell

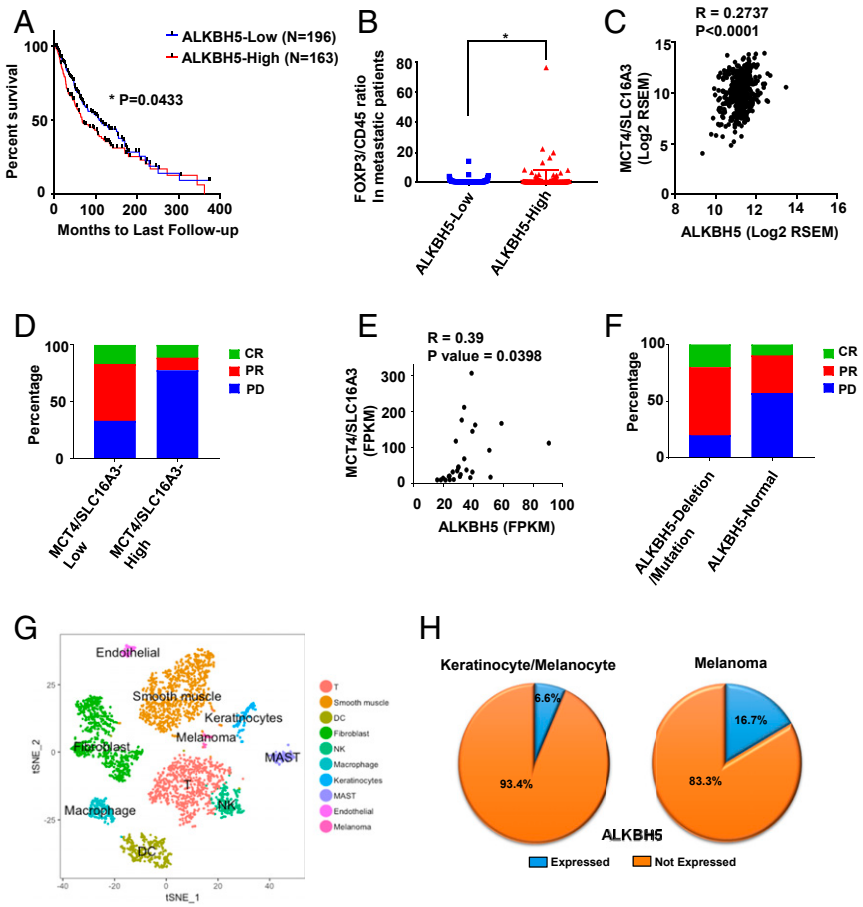

Fig. 5. ALKBH5 expression influences the response of melanoma patients to anti–PD-1 therapy. (*A*) Kaplan–Meier survival rate analysis of TCGA metastasized melanoma patients grouped by ALKBH5 mRNA levels. Patients with follow-up history were included in the analysis; the mean ALKBH5 level for the entire group was used as the cut-off value. ALKBH5 low: $n = 196$; ALKBH5 high: $n = 163$. (*B*) FOXP3/CD45 expression ratio was calculated for metastatic melanoma patients grouped by ALKBH5 mRNA levels; the mean ALKBH5 level for the entire group was used as the cut-off value. ALKBH5 low: $n = 196$; ALKBH5 high: $n = 163$. $^*P < 0.05$. (*C*) Pearson correlation of ALKHB5 and SLC16A3/MCT4 in melanoma patients from the TCGA database ($n = 472$). (*D*) Melanoma patients ($n = 26$) carrying low or high MCT4/SLC16A3 mRNA expression were treated with pembrolizumab or nivolumab anti–PD-1 Ab. Average expression was used as cut-off. The percentage with complete response (CR), partial response (PR), and progressive disease (PD) are shown. Data are from GSE78220. (*E*) Pearson correlation of ALKHB5 and MCT4/SLC16A3 in melanoma patients treated with pembrolizumab or nivolumab anti–PD-1 Ab (GSE78220). (*F*) Melanoma patients carrying wild-type (normal) or deleted/mutated ALKHB5 gene were treated with pembrolizumab or nivolumab. complete response (CR), partial response (PR), and progressive disease (PD) are shown (GSE78220). (*G*) scRNA-seq data presented as *t*-distributed stochastic neighbor embedding (t-SNE) plots. Cells were from a tumor biopsy collected from a melanoma patient who showed a response to anti–PD-1 therapy. Plots show the distribution of identified cells. (*H*) ALKBH5 expression in normal keratinocytes/melanocytes and melanoma tumor cells in melanoma patient receiving PD-1 therapy. See also *SI Appendix*, Fig. S10.

types in the tumor (Fig. 5*G*), with substantial immune cell infiltration and very few residual melanoma cells, reflecting the response to therapy. We then examined ALKBH5 expression in the tumor cells and found that 16.7% of melanoma cells (16.7%) expressed ALKBH5 compared with only 6.6% of normal keratinocytes and melanocytes surrounding the tumor cells (Fig. 5*H*). Taken together, these results indicate that tumor expression of ALKBH5 might be a predictive biomarker of patient's survival and response to anti–PD-1 therapy, at least for melanoma patients.

A Small-Molecule Inhibitor of Alkbh5 Enhances the Efficacy of Anti–PD-1 Therapy. Our results thus far indicate that loss of m^6A demethylase Alkbh5, in B16 melanoma cells, potentiates the efficacy of GVAX/anti–PD-1 therapy. To identify clinically relevant pharmacological inhibitors of Alkbh5, we have identified a specific inhibitor of ALKBH5, named ALK-04, by in silico screening of compounds using the X-ray crystal structure of ALKBH5 (PDB ID code 4NRO) and by performing structure–activity relationship studies on a library of synthesized compounds. First, we tested the cytotoxicity of the inhibitor in vitro, and B16 cells proliferation was not significantly affected by inhibitor treatment (Fig. 6*A*). Next, we compared tumor growth of control and inhibitor-treated mice during immunotherapy. Consistent with our previous findings of Alkbh5-KO tumor, mice treated with ALKBH5 inhibitor significantly reduced tumor growth compared to control (Fig. 6*B* and *SI Appendix*, Fig. S10*A*). These results confirmed the function of Alkbh5 in restricting the efficacy of immunotherapy and provide a rational for future combinatorial therapy by using an ALKBH5 inhibitor.

Discussion

A major challenge facing the future of ICB for cancer is to understand the mechanisms of resistance to ICB and to develop combination therapies that enhance antitumor immunity and durable responses. Using the poorly immunogenic B16 mouse model of melanoma, which is resistant to ICB, we discovered that genetic inactivation of the demethylases Alkbh5 and Fto in tumor cells rendered them more susceptible to anti–PD-1/GVAX therapy. The possibility that a similar approach could be employed for clinical applications is supported by the finding that Alkbh5 and Fto KO mice are viable (7, 8). This contrasts with m^6A methyltransferases, which are known to be essential for embryonic development and stem cell differentiation (50, 51). Notably, a recent study showed that anti–PD-1 blockade responses were enhanced in FTO knockdown tumors (21). We also observed a similar trend with FTO-KO tumors during PD-1 Ab treatment, but it is not as robust as observed for Alkbh5-KO tumors (Fig. 1 and *SI Appendix*, Fig. S1). Therefore, Alklbh5 has more obvious effects on PD-1 Ab treatment alone or combined with GVAX compared to Fto (Fig. 1). Besides, it seems that the role of FTO in cell proliferation dominates the effects of FTO for in vivo tumor growth from the published report (21), which we did not observe in our experiments (*SI Appendix*, Fig. S1 *M–O*). Overall, our data showed a more dramatic effects of Alkbh5 in regulating immunotherapy compared to Fto, and we further dissected the mechanisms of Alkbh5 in this process.

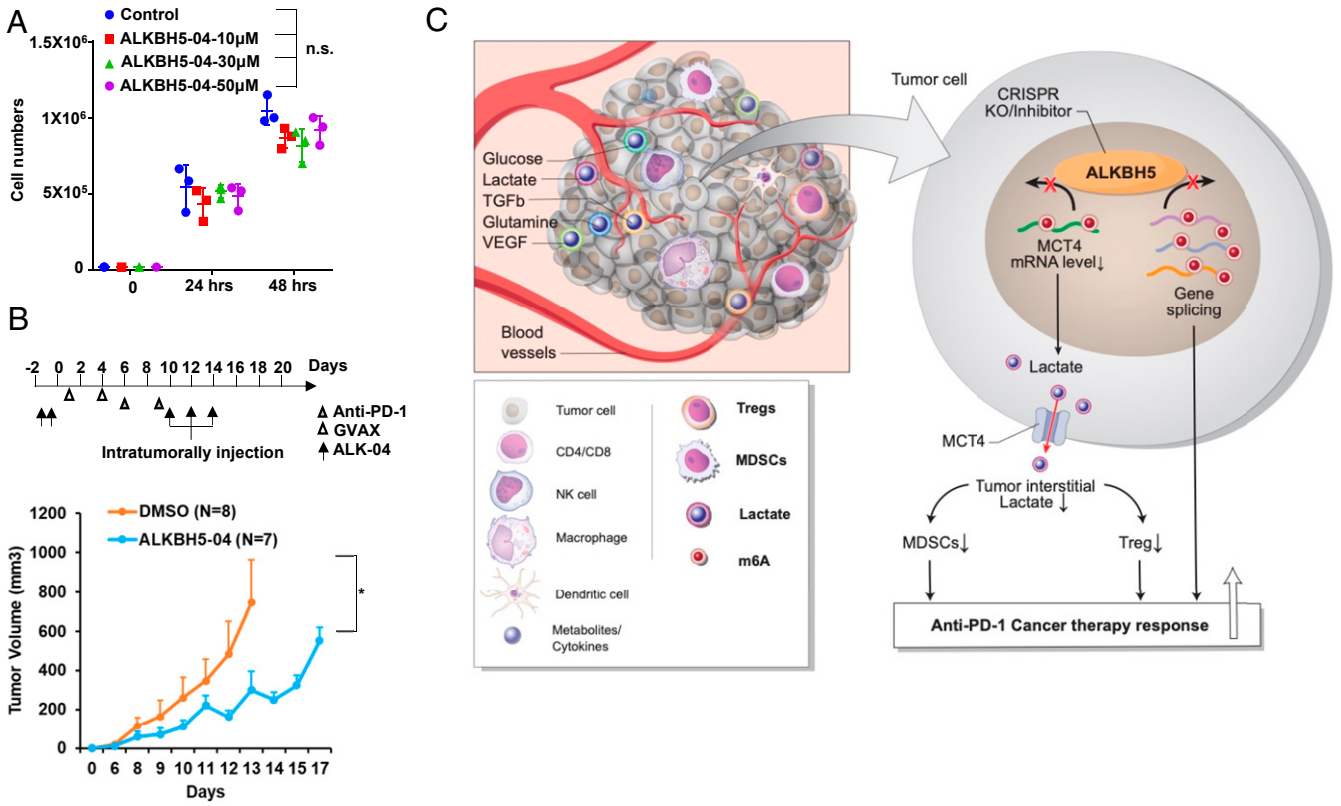

Fig. 6. ALKBH5 inhibitor enhances efficacy of immunotherapy in combination with GVAX and PD-1 Ab. (*A*) Proliferation assay of B16 cells treated with DMSO control and 10 μM, 30 μM, and 50 μM ALKBH5 inhibitor. (*B*) Treatment timeline and mouse B16 tumor growth of control and ALKHB5 inhibitor combined with PD-1 and GVAX immunotherapy. $*P < 0.05$. (*C*) Proposed model for ALKBH5-mediated regulation of immunotherapy. ALKBH5 influences anti–PD-1 therapy responses by modifying m^6A levels and splicing of specific genes. Inhibition of ALKBH5 mRNA demethylation by CRISPR or a small molecule increased m^6A on MCT4/SLC16A3, a lactate transporter, which reduced its mRNA levels leading to reduction of lactate in TIFs. Consequently, MDSC and Treg suppressive immune cell populations in the TME are decreased and immunotherapy therapy responses are enhanced. See *Results* section for details.

Tregs and MDSCs are the dominant immunosuppressive cell populations in antitumor immunity (27). In our study, we found that both cell populations were reduced in Alkbh5-KO tumors during GVAX/anti–PD-1 therapy, whereas the abundance of DCs increased. A decrease in tumor infiltration of MDSCs and Tregs was also observed in a mouse model of 4T1 tumors in response to the anti–PD-1/anti–CTLA-4 plus AZA/ENT treatment (23). Importantly, here we propose the link between m^6A demethylase ALKBH5 and the altered tumor infiltrated lymphocytes composition during anti–PD-1/GVAX immunotherapy, providing a new target to regulate the mechanism of the TME and modulate of immunotherapy outcomes.

Our results showed that the function of Alkbh5 in regulating the TME and immunotherapy efficacy was not through the IFN-γ pathway, in accordance with the observation of unchanged infiltrated cytotoxic CD8 T cell population in Alkbh5-deficient tumors. Instead, Alkbh5 KO increased the m^6A density in its targets and decreased mRNA expression or enhanced percentage of exon splice-in ratios. For example, Mex3d and Mct4/Slc16a3 mRNA expression was reduced in Alkhb5-KO tumors compared with NTC tumors during GVAX/anti–PD-1 therapy. Mex3d is an RNA-binding protein with putative roles in RNA turnover (52), and Mct4/Slc16a3 is important for pH maintenance, lactate secretion, and nonoxidative glucose metabolism in cancer cells (53). Reduced lactate concentration in the TME has been linked to impaired MDSC and Treg expansion and differentiation (46, 47). In this study, we found that Alkbh5 enzymatic activity is indispensable for regulating in vivo tumor growth during GVAX/anti–PD-1 therapy. Mct4/Slc16a3 was one of the major targets of Alkbh5 during this process. Alkbh5-KO B16 tumors displayed reductions in Mct4/Slc16a3 expression, lactate content in TIF, and MDSC and Treg abundance in the TME. Rescue experiments showed that Mct4/Slc16a3 was responsible for regulating lactate concentration and MDSC, Treg accumulation in Alkbh5-KO tumors during the GVAX/anti–PD-1 therapy. In addition, Mct4/Slc16a3 was reported to regulate VEGF expression in tumor cells (54). We also observed a reduction in the TME level of Vegfα in Alkbh5-KO tumors (Fig. 4*B* and *SI Appendix*, Fig. S6*H*).

Except for Mct4, we also analyzed several genes with altered PSI in the Mct4-expressing Alkbh5-KO cells. Gene splicing did not change in the rescue cells compared with Alkbh5-KO cells (Fig. 4*J* and *SI Appendix*, Fig. S7 *C–E*); these results suggest that gene splicing may play a role independent of Mct4. Previous studies have shown that tumor-specific alternative splicing-derived neoepitopes were related to immunotherapy response (55). We examined the gene-mutation profiles of several of those genes with altered PSI in melanoma patients, and indeed we found that these genes harbored the mutations that affected gene splicing in patients (*SI Appendix*, Fig. S7*F*). The extract role and detailed mechanisms of gene splicing in Alkbh5-KO tumors during GVAX/anti–PD-1 therapy will need further investigations.

In summary, we have uncovered a previously unknown function for tumor-expressed Alkbh5 in regulating metabolite/cytokine content and filtration of immune cells in the TME during GVAX/anti–PD-1 therapy. Alkbh5-mediated alterations in the density of m^6A was found to regulate the splicing and expression of mRNAs with potential roles in the control of tumor growth (Fig. 6*C*). These findings highlight the importance of m^6A demethylation in regulating the tumor response to immunotherapy and suggest that ALKBH5 could be a potential therapeutic target, alone or in combination with ICB, for cancer.

Materials and Methods

Tumor samples were obtained from a melanoma patient who had been treated with anti–PD-1 Ab. The procedures were approved by the University of California San Diego Institutional Review Board and the patient provided informed consent. Animal studies and procedures were approved by the University of California San Diego Institutional Animal Care and Use Committee. Details of materials regarding cell lines, mouse strains and human tumor specimens, antibodies, and reagents used for our study can be found in *SI Appendix*. Detailed methods of mouse models and treatments, CRISPR/Cas9-mediated generation of KO cell lines, flow cytometry analysis of tumor-infiltrating immune cells, qRT-PCR and RNA-seq, MeRIP-seq, MeRIP-seq data analysis, alternative splicing and splice junction analysis, scRNA-seq of human melanoma specimens, TIF isolation and analysis, IFN-γ stimulation of melanoma cells in vitro, cell proliferation assay, Western blot analysis, immunohistochemistry, and LC-MS/MS analysis of m^6A RNA can also be found in *SI Appendix*.

Data Availability. The data reported in this paper have been deposited in the Gene Expression Omnibus (GEO) database, https://www.ncbi.nlm.nih.gov/geo (accession no. GSE134388).

ACKNOWLEDGMENTS. We thank Drs. Glenn Dranoff and Michael Dougan for providing the B16 (GVAX) cells; Dr. Kristen Jepsen of the Institute of Genomic Medicine at the University of California San Diego (UCSD) for help with the high-throughput sequencing; Dr. Neal Sekiya and Ms. Tara Rambaldo at the Center for AIDS Research at UCSD for flow cytometry analysis; the UCSD Histology and Immunohistochemistry Core for help with tissue analysis; and members of the T.M.R. laboratory for helpful discussions and advice. This publication includes data generated at the UC San Diego IGM Genomics Center utilizing an Illumina NovaSeq 6000 that was purchased with funding from a National Institutes of Health SIG grant (#S10 OD026929). This work was supported in part by grants from the National Institutes of Health (CA177322, DA039562, DA046171, and AI 125103).

1. D. S. Chen, I. Mellman, Elements of cancer immunity and the cancer-immune set point. *Nature* **541**, 321–330 (2017).
2. K. D. Meyer, S. R. Jaffrey, Rethinking m^6A readers, writers, and erasers. *Annu. Rev. Cell Dev. Biol.* **33**, 319–342 (2017).
3. H. Shi, J. Wei, C. He, Where, when, and how: Context-dependent functions of RNA methylation writers, readers, and erasers. *Mol. Cell* **74**, 640–650 (2019).
4. K. D. Meyer *et al.*, Comprehensive analysis of mRNA methylation reveals enrichment in 3′ UTRs and near stop codons. *Cell* **149**, 1635–1646 (2012).
5. D. Dominissini *et al.*, Topology of the human and mouse m6A RNA methylomes revealed by m6A-seq. *Nature* **485**, 201–206 (2012).
6. S. Schwartz *et al.*, Perturbation of m6A writers reveals two distinct classes of mRNA methylation at internal and 5′ sites. *Cell Rep.* **8**, 284–296 (2014).
7. G. Jia *et al.*, N6-methyladenosine in nuclear RNA is a major substrate of the obesity-associated FTO. *Nat. Chem. Biol.* **7**, 885–887 (2011).
8. G. Zheng *et al.*, ALKBH5 is a mammalian RNA demethylase that impacts RNA metabolism and mouse fertility. *Mol. Cell* **49**, 18–29 (2013).
9. J. Mauer *et al.*, Reversible methylation of m^6A_m in the 5′ cap controls mRNA stability. *Nature* **541**, 371–375 (2017).
10. J. Mauer *et al.*, FTO controls reversible m^6Am RNA methylation during snRNA biogenesis. *Nat. Chem. Biol.* **15**, 340–347 (2019).
11. D. P. Patil, B. F. Pickering, S. R. Jaffrey, Reading m^6A in the transcriptome: m^6A-Binding proteins. *Trends Cell Biol.* **28**, 113–127 (2018).
12. X. Wang, C. He, Reading RNA methylation codes through methyl-specific binding proteins. *RNA Biol.* **11**, 669–672 (2014).
13. Y. Yang, P. J. Hsu, Y. S. Chen, Y. G. Yang, Dynamic transcriptomic m^6A decoration: Writers, erasers, readers and functions in RNA metabolism. *Cell Res.* **28**, 616–624 (2018).
14. H. B. Li *et al.*, m^6A mRNA methylation controls T cell homeostasis by targeting the IL-7/STAT5/SOCS pathways. *Nature* **548**, 338–342 (2017).
15. S. R. Gonzales-van Horn, P. Sarnow, Making the mark: The role of adenosine modifications in the life cycle of RNA viruses. *Cell Host Microbe* **21**, 661–669 (2017).
16. I. Barbieri *et al.*, Promoter-bound METTL3 maintains myeloid leukaemia by m^6A-dependent translation control. *Nature* **552**, 126–131 (2017).
17. D. Han *et al.*, Anti-tumour immunity controlled through mRNA m^6A methylation and YTHDF1 in dendritic cells. *Nature* **566**, 270–274 (2019).
18. J. Paris *et al.*, Targeting the RNA m^6A reader YTHDF2 selectively compromises cancer stem cells in acute myeloid leukemia. *Cell Stem Cell* **25**, 137–148.e6 (2019).
19. R. Su *et al.*, R-2HG exhibits anti-tumor activity by targeting FTO/m^6A/MYC/CEBPA signaling. *Cell* **172**, 90–105.e23 (2018).
20. L. P. Vu *et al.*, The N^6-methyladenosine (m^6A)-forming enzyme METTL3 controls myeloid differentiation of normal hematopoietic and leukemia cells. *Nat. Med.* **23**, 1369–1376 (2017).
21. S. Yang *et al.*, m^6A mRNA demethylase FTO regulates melanoma tumorigenicity and response to anti-PD-1 blockade. *Nat. Commun.* **10**, 2782 (2019).
22. R. T. Manguso *et al.*, In vivo CRISPR screening identifies Ptpn2 as a cancer immunotherapy target. *Nature* **547**, 413–418 (2017).
23. K. Kim *et al.*, Eradication of metastatic mouse cancers resistant to immune checkpoint blockade by suppression of myeloid-derived cells. *Proc. Natl. Acad. Sci. U.S.A.* **111**, 11774–11779 (2014).

24. T. H. Corbett, D. P. Griswold Jr., B. J. Roberts, J. C. Peckham, F. M. Schabel Jr., Tumor induction relationships in development of transplantable cancers of the colon in mice for chemotherapy assays, with a note on carcinogen structure. *Cancer Res.* **35**, 2434–2439 (1975).
25. L. P. Belnap, P. H. Cleveland, M. E. Colmerauer, R. M. Barone, Y. H. Pilch, Immunogenicity of chemically induced murine colon cancers. *Cancer Res.* **39**, 1174–1179 (1979).
26. G. Dranoff, GM-CSF-secreting melanoma vaccines. *Oncogene* **22**, 3188–3192 (2003).
27. T. Fujimura, Y. Kambayashi, S. Aiba, Crosstalk between regulatory T cells (Tregs) and myeloid derived suppressor cells (MDSCs) during melanoma growth. *OncoImmunology* **1**, 1433–1434 (2012).
28. Y. Y. Setiady, J. A. Coccia, P. U. Park, In vivo depletion of CD4+FOXP3+ Treg cells by the PC61 anti-CD25 monoclonal antibody is mediated by FcgammaRIII+ phagocytes. *Eur. J. Immunol.* **40**, 780–786 (2010).
29. F. Arce Vargas *et al*.; Melanoma TRACERx Consortium; Renal TRACERx Consortium; Lung TRACERx Consortium, Fc-optimized anti-CD25 depletes tumor-infiltrating regulatory T cells and synergizes with PD-1 blockade to eradicate established tumors. *Immunity* **46**, 577–586 (2017).
30. W. Hugo *et al*., Genomic and transcriptomic features of response to anti-PD-1 therapy in metastatic melanoma. *Cell* **165**, 35–44 (2016).
31. H. Weng *et al*., METTL14 inhibits hematopoietic stem/progenitor differentiation and promotes leukemogenesis via mRNA m^6A modification. *Cell Stem Cell* **22**, 191–205.e9 (2018).
32. B. Linder *et al*., Single-nucleotide-resolution mapping of m6A and m6Am throughout the transcriptome. *Nat. Methods* **12**, 767–772 (2015).
33. G. Lichinchi, T. M. Rana, Profiling of N^6-methyladenosine in zika virus RNA and host cellular mRNA. *Methods Mol. Biol.* **1870**, 209–218 (2019).
34. G. Lichinchi *et al*., Dynamics of human and viral RNA methylation during zika virus infection. *Cell Host Microbe* **20**, 666–673 (2016).
35. G. Lichinchi *et al*., Dynamics of the human and viral m(6)A RNA methylomes during HIV-1 infection of T cells. *Nat. Microbiol.* **1**, 16011 (2016).
36. A. Louloupi, E. Ntini, T. Conrad, U. A. V. Ørom, Transient N-6-Methyladenosine transcriptome sequencing reveals a regulatory role of m6A in splicing efficiency. *Cell Rep.* **23**, 3429–3437 (2018).
37. S. Ke *et al*., m^6A mRNA modifications are deposited in nascent pre-mRNA and are not required for splicing but do specify cytoplasmic turnover. *Genes Dev.* **31**, 990–1006 (2017).
38. C. Tang *et al*., ALKBH5-dependent m6A demethylation controls splicing and stability of long 3′-UTR mRNAs in male germ cells. *Proc. Natl. Acad. Sci. U.S.A.* **115**, E325–E333 (2018).
39. T. Condamine, I. Ramachandran, J. I. Youn, D. I. Gabrilovich, Regulation of tumor metastasis by myeloid-derived suppressor cells. *Annu. Rev. Med.* **66**, 97–110 (2015).
40. A. Matsumura *et al*., HGF regulates VEGF expression via the c-Met receptor downstream pathways, PI3K/Akt, MAPK and STAT3, in CT26 murine cells. *Int. J. Oncol.* **42**, 535–542 (2013).
41. G. Neufeld, A. D. Sabag, N. Rabinovicz, O. Kessler, Semaphorins in angiogenesis and tumor progression. *Cold Spring Harb. Perspect. Med.* **2**, a006718 (2012).
42. G. Villain *et al*., miR-126-5p promotes retinal endothelial cell survival through SetD5 regulation in neurons. *Development* **145**, dev156232 (2018).
43. Y. Kotani *et al*., Alternative exon skipping biases substrate preference of the deubiquitylase USP15 for mysterin/RNF213, the moyamoya disease susceptibility factor. *Sci. Rep.* **7**, 44293 (2017).
44. S. Pilotto *et al*., MET exon 14 juxtamembrane splicing mutations: Clinical and therapeutical perspectives for cancer therapy. *Ann. Transl. Med.* **5**, 2 (2017).
45. M. Wagner, H. Wiig, Tumor interstitial fluid formation, characterization, and clinical implications. *Front. Oncol.* **5**, 115 (2015).
46. Z. Husain, P. Seth, V. P. Sukhatme, Tumor-derived lactate and myeloid-derived suppressor cells: Linking metabolism to cancer immunology. *OncoImmunology* **2**, e26383 (2013).
47. A. Angelin *et al*., Foxp3 reprograms T cell metabolism to function in low-glucose, high-lactate environments. *Cell Metab.* **25**, 1282–1293.e7 (2017).
48. C. Feng *et al*., Crystal structures of the human RNA demethylase Alkbh5 reveal basis for substrate recognition. *J. Biol. Chem.* **289**, 11571–11583 (2014).
49. D. Pan *et al*., A major chromatin regulator determines resistance of tumor cells to T cell-mediated killing. *Science* **359**, 770–775 (2018).
50. S. Geula *et al*., Stem cells. m6A mRNA methylation facilitates resolution of naïve pluripotency toward differentiation. *Science* **347**, 1002–1006 (2015).
51. T. G. Meng *et al*., Mettl14 is required for mouse postimplantation development by facilitating epiblast maturation. *FASEB J.* **33**, 1179–1187 (2019).
52. K. Buchet-Poyau *et al*., Identification and characterization of human Mex-3 proteins, a novel family of evolutionarily conserved RNA-binding proteins differentially localized to processing bodies. *Nucleic Acids Res.* **35**, 1289–1300 (2007).
53. F. Baenke *et al*., Functional screening identifies MCT4 as a key regulator of breast cancer cell metabolism and survival. *J. Pathol.* **237**, 152–165 (2015).
54. Q. Sun, L. L. Hu, Q. Fu, MCT4 promotes cell proliferation and invasion of castration-resistant prostate cancer PC-3 cell line. *EXCLI J.* **18**, 187–194 (2019).
55. L. Frankiw, D. Baltimore, G. Li, Alternative mRNA splicing in cancer immunotherapy. *Nat. Rev. Immunol.* **19**, 675–687 (2019).